Published in final edited form as:
Structure. 2013 March 5; 21(3): 342–354. doi:10.1016/j.str.2013.01.004.

The Structure of the Tiam1 PDZ Domain/Phospho-Syndecan1 Complex Reveals a Ligand Conformation that Modulates Protein Dynamics

Xu Liu[1,3], **Tyson R. Shepherd**[1,3,4], **Ann M. Murray**[1], **Zhen Xu**[1], and **Ernesto J. Fuentes**[1,2,*]

[1]Department of Biochemistry, University of Iowa, Carver College of Medicine, Iowa City, IA 52242, USA

[2]Holden Comprehensive Cancer Center, University of Iowa, Carver College of Medicine, Iowa City, IA 52242, USA

SUMMARY

PDZ (PSD-95/Dlg/ZO-1) domains are protein-protein interaction modules often regulated by ligand phosphorylation. Here, we investigated the specificity, structure, and dynamics of Tiam1 PDZ domain/ligand interactions. We show that the PDZ domain specifically binds syndecan1 (SDC1), phosphorylated SDC1 (pSDC1), and SDC3 but not other syndecan isoforms. The crystal structure of the PDZ/SDC1 complex indicates that syndecan affinity is derived from amino acids beyond the four C-terminal residues. Remarkably, the crystal structure of the PDZ/pSDC1 complex reveals a binding pocket that accommodates the phosphoryl group. Methyl relaxation experiments of PDZ/SCD1 and PDZ/pSDC1 complexes reveal that PDZ-phosphoryl interactions dampen dynamic motions in a distal region of the PDZ domain by decoupling them from the ligand-binding site. Our data are consistent with a selection model by which specificity and phosphorylation regulate PDZ/syndecan interactions and signaling events. Importantly, our relaxation data demonstrate that PDZ/phospho-ligand interactions regulate protein dynamics and their coupling to distal sites.

INTRODUCTION

T cell lymphoma invasion and metastasis 1 (Tiam1) is a guanine nucleotide exchange factor (GEF) that activates the Rho-family GTPase Rac1. This multidomain protein is important for both cell-cell junction integrity (Malliri et al., 2004; Mertens et al., 2005; Nishimura et al., 2005; Zhang and Macara, 2006) and cell-matrix interactions (Malliri et al., 2004;

*Correspondence: ernesto-fuentes@uiowa.edu.
[3]These authors contributed equally to this work
[4]Present address: Department of Cell and Molecular Biology, Uppsala University, 75124 Uppsala, Sweden

ACCESSION NUMBERS

The atomic coordinates and structure factor amplitudes have been deposited in the PDB with accession codes 4GVD and 4GVC for the SDC1- and pSDC1-bound PDZ domains, respectively.

SUPPLEMENTAL INFORMATION

Supplemental Information includes Supplemental Experimental Procedures, two tables, and five figures and can be found with this article online at http://dx.doi.org/10.1016/j.str.2013.01.004.

Masuda et al., 2010; Shepherd et al., 2010). In vivo, the spatial and temporal function of Tiam1 is regulated by protein-protein interaction domains, including the PSD-95/Dlg/ZO-1 (PDZ) domain. PDZ domains are small (~90 amino acids) and typically bind the 4–10 carboxy-terminal residues of partner proteins. We have shown that the PDZ domain of Tiam1 binds the C terminus of syndecan1 (SDC1) and that this interaction is important for cell-matrix adhesion and cell motility (Shepherd et al., 2010).

The syndecan family of cell-surface heparan-sulfate proteoglycans has four members, SDC1–4, whose extracellular domains interact with a variety of ligands, such as integrin, fibronectin, laminin, and growth factors. The C-terminal cytoplasmic domain is divided into two highly conserved (C1 and C2) regions separated by a variable (V) region (Couchman, 2010). The C2 region binds the PDZ domains of syntenin1 (Zimmermann et al., 2001), synectin1 (or GIPC1) (Gao et al., 2000), synbindin (Ethell et al., 2000), CASK (or LIN-2) (Cohen et al., 1998), and Tiam1 (Shepherd et al., 2010). However, the specificity of each of these PDZ domains for particular syndecan family members remains unknown. SDC1, SDC3, and SDC4 are tyrosine phosphorylated (by unknown Src tyrosine kinases) within their respective cytoplasmic domains, which is critical for downstream signaling (Asundi and Carey, 1997; Ott and Rapraeger, 1998). In the case of SDC1, phosphorylation of the PDZ-binding motif regulates the switch between cell adhesion and ectodomain cleavage by disrupting phosphorylated SDC1 (pSDC1) interactions with the second PDZ domain of syntenin1 (Reiland et al., 1996; Sulka et al., 2009). The exact location(s) and biological consequences of SDC3 and SDC4 phosphorylation remain unknown. Interestingly, we have reported that pSDC1 binds to the Tiam1 PDZ domain with an affinity similar to that of unphosphorylated SDC1, suggesting that phosphorylation also plays a role in selecting SDC1 binding partners (Shepherd et al., 2010). Although many examples of positive PDZ/ligand regulation by phosphorylation have emerged, the physical basis for this phenomenon remains unexplored.

The structures of many apo and ligand-bound PDZ domain pairs have been determined (see Lee and Zheng, 2010), and in most cases, there is very little change in the overall domain structure after ligand binding. However, nuclear magnetic resonance (NMR) spin relaxation and computational analyses have revealed changes in the intrinsic dynamics of PDZ domains (De Los Rios et al., 2005; Dhulesia et al., 2008; Fuentes et al., 2004; Kong and Karplus, 2009). Upon ligand binding, energetic and dynamic changes are propagated from the ligand-binding site to distal regions of the PDZ domain via intramolecular allosteric communication pathway(s) (Fuentes et al., 2004, 2006; Lockless and Ranganathan, 1999; Petit et al., 2009). This long-range allostery is not only of structural and thermodynamic interest but also of biological significance. For example, in the case of the Par6 protein, which contains a PDZ domain and Cdc42/Rac1 interactive-binding (CRIB) motif, binding of Cdc42 to the CRIB motif allosterically modulates the energetics of PDZ interactions through a conformational switch mechanism (Whitney et al., 2011). More generally, it is clear that protein dynamics have a role in both allostery and the affinity of ligand binding (Marlow et al., 2010; Tzeng and Kalodimos, 2011). However, the relationships between ligand affinity, protein dynamics, and allostery are not well understood and currently the topic of intensive study.

Here, we determined the energetic and structural basis for Tiam1 PDZ domain interactions with syndecan proteins and the impact of phosphorylation on protein dynamics. We present the crystal structures of the Tiam1 PDZ domain in complex with SDC1 and pSDC1. Remarkably, these structures show that the PDZ domain recognizes a conformation of the phosphotyrosine residue in the absence of significant structural changes in the PDZ domain. NMR-based methyl side-chain relaxation experiments of three PDZ/ligand complexes reveal distinct patterns of dynamics. Collectively, we report the structure of a PDZ/phospho-ligand and show that the phosphoryl moiety is critical for regulating PDZ domain dynamics.

RESULTS

The Tiam1 PDZ Domain Has a Binding Preference for SDC1 and SDC3

Our previous work indicated that ligand residues beyond the C-terminal four contribute to Tiam1 PDZ domain binding affinity and that this domain binds SDC1 and pSDC1 (Shepherd et al., 2010). Examination of the C termini of the four syndecan isoforms revealed differences in amino-acid sequence that may be critical for defining specificity in PDZ domain interactions (Figure 1A). We tested this idea by synthesizing fluorescently labeled peptides corresponding to the final eight residues of SDC2–4 and measuring their affinity for the Tiam1 PDZ domain. Binding by SDC3 had reasonable affinity (K_d ~30 μM), whereas that of SDC2 and SDC4 was more than 15-fold weaker (K_ds ≥ 400 μM; Figure 1B; Table 1). Isothermal titration calorimetry (ITC) data agree well with the fluorescence binding data for SDC1 and pSDC1 but indicate that the dansyl group nonspecifically increases binding affinity <2-fold (Figure 2; Supplemental Experimental Procedures available online), as previously noted for other PDZ domains (Harris et al., 2001; Kang et al., 2003).

Tiam1 PDZ/SDC1 Specificity Is Determined by Two Binding Pockets

We investigated the physical basis for PDZ/syndecan interactions by solving the crystal structure of the Tiam1 PDZ domain bound to a C-terminal SDC1 peptide. The structure of the Tiam1 PDZ/SDC1 complex was solved to 1.85 Å resolution (Table 2). The PDZ domain has five β strands and two α helices arranged in a β barrel fold with the ligand-binding site contained within a groove formed by residues in the β2 strand and the α2 helix. The entire SDC1 peptide interacts with residues along the PDZ β2 strand (residues 858–866), as well as with two specificity pockets (Figure 3A). The S_0 pocket is formed by the side chains of residues Y858, F860, and L915 and accommodates the alanine side chain at the C-terminal position (P_0) of SDC1, whereas the $S^{-}{}_2$ pocket is formed by the side chains of L911 and K912 and accommodates the $P^{-}{}_2$ phenylalanine side chain of SDC1 (Figure 3C).

In addition to showing the typical β sheet PDZ/ligand interactions, the structure demonstrates that N-terminal residues of the SDC1 peptide participate in specific interactions. For example, the P_{-3} glutamate and P_{-6} lysine form a hydrogen bond network with the P_{-1} tyrosine hydroxyl and the N876 side chain of the PDZ domain (Figure 3). Moreover, an interaction between the side chains of the P_{-4} glutamate and K912 of the PDZ domain is apparent. Although the electron density of the side chain of the P_{-4} glutamate was not visualized beyond the β-carbon atom, model building indicates that the closest approach of its oxygens (OE1/2) to the K912 nitrogen (NZ) is ~5 Å. To determine the significance of

this ion pair in stabilizing the PDZ/SDC1 interaction, we generated mutations in the PDZ domain (PDZ-K912E) and SDC1 peptide (SDC1-EP_4K). The affinity of each for its wild-type partner was reduced (~4- and 5-fold, respectively), whereas the affinity of the mutant PDZ-K912E/SDC1- $EP_{-4}K$ pair was even lower (~13-fold reduction; Table 1). Double-mutant cycle analysis indicated that the K912 and EP_{-4} side chains were energetically coupled but not to the level found in stable salt bridges ($\Delta\Delta\Delta G_{INT}$ = 0.22 ± 0.14 kcal/mol compared to ~0.7 kcal/mol; Table S1) (Makhatadze et al., 2003). This suggests that the electrostatic interaction between PDZ-K912 and SDC1-EP_{-4} is not persistent over time; rather, it is stable for only a fraction of the time resulting in a transient electrostatic interaction. This finding is supported by our previous study, showing that mutation of a model peptide from E to K at P_{-4}, as found in SDC2, reduced the affinity for the wild-type PDZ domain ~5-fold (Shepherd and Fuentes, 2011). Together, these data suggest that, although important, the EP_{-4} and K912 interaction is not the sole determinant of the differences in binding affinity seen with SDC-family peptides.

The Structure of the Tiam1 PDZ/pSDC1 Complex Reveals a Phosphotyrosine Binding Pocket

Given that the affinity of the Tiam1 PDZ domain for SDC1 and pSDC1 are similar (Table 1) and no structure of a PDZ domain in complex with a phosphorylated ligand has been reported, we determined the crystal structure of the Tiam1 PDZ/pSDC1 complex (1.54 Å resolution; Table 2). A comparison of the PDZ domain backbone in the SDC1 and pSDC1 structures revealed a root-mean-square deviation (rmsd) of ~0.26 Å, indicating that ligand binding does not lead to significant rearrangement of the PDZ domain. Moreover, NMR-based ^{15}N-HSQC titration experiments showed that chemical shift changes in the PDZ domain upon binding either ligand were nearly identical, indicating minimal structural changes in the PDZ domain (Figure S2). In contrast, the three-dimensional structure showed that the pSDC1 phosphotyrosine was rotated ~90° into a groove formed by α1 helix and the β1-β2 loop (Figures 3 and 4). This conformation is stabilized by interactions between the phosphoryl adduct and the side-chain amine of K879 (α1 helix) and the hydroxyl group of T857 (β1-β2 loop) in the PDZ domain. To test the importance of residue K879 in the PDZ/pSDC1 interaction, we constructed a double-mutant thermodynamic cycle using PDZ-WT, PDZ-K879E, SDC1, and pSDC1. The interactions of PDZ-K879E with SDC1 and pSDC1 peptides had K_ds that were 2- and 9-fold weaker, respectively, than those for PDZ-WT (Table 1). Double-mutant cycle analysis revealed that the phosphoryl group and the K879 side chain were energetically coupled ($\Delta\Delta\Delta G_{INT}$ = 0.83 ± 0.05 kcal/mol) (Table S1).

Ligand Binding Results in Uniform Changes in Backbone Dynamics

Previously, we determined that C termini of the adhesion proteins SDC1, pSDC1, and Caspr4 bind the Tiam1 PDZ domain with affinities ranging from 17–26 μM (Shepherd et al., 2010). To determine the extent of the changes in dynamics along the backbone for the Tiam1 PDZ domain upon complexing with the three ligands, we performed ^{15}N-based relaxation analyses, obtaining an order parameter (S^2) and timescale of motion (τ_e) for each amide. In the absence of peptide ligand, we were able to analyze 81 of 88 nonproline backbone-amide residues in the PDZ domain. In regions of defined secondary structure, amide motions were highly restricted, with an average S^2 of 0.86 (Figure 5). In contrast,

residues in the β1-β2 loop (residues 851–858), β2-β3 loop (residues 866–872), and β5-α2 loop (residues 904–909) were more dynamic (average S^2 = 0.73) (Figure 5A). In addition, residues in helix α2 (residues 906 and 912–917) displayed chemical exchange (R_{ex}), and residues 908 and 909 were broadened beyond detection indicating milli- to microsecond motions (Figures S3 and S4). In analyzing the Tiam1 PDZ/SDC1, PDZ/pSDC1, and PDZ/Caspr4 complexes, we deemed changes in dynamics relative to the free PDZ domain (ΔS^2, $\Delta\tau_e$, or ΔR_{ex}) significant if the calculated difference in that parameter was 1.5-fold greater than the propagated error. Overall, only small changes in dynamics occurred in all three complexes but upon binding their respective ligands the dynamics response of the three complexes was similar—residues in the β1-β2 loop, β2 strand (859–865), and α2 helix (residues 911, 912, and 915) had more restricted motions (Figures 5 and S3).

Ligand Binding Modulates PDZ Domain Side-Chain Dynamics

To determine how distinct ligands (SDC1, pSDC1, and Caspr4) affect PDZ domain side-chain dynamics, we employed ^{2}H relaxation experiments to characterize the pico- to nanosecond timescale motions of methyl groups. The methyl-axis order parameter (S^2_{axis}) and τ_e were determined using the model-free formalism. S^2_{axis} represents the amplitude of the motion of the bond along the axis of symmetry of the methyl group (C-CH_3), and τ_e represents the timescale of its reorientation. Changes in S^2_{axis} and/or τ_e (ΔS^2_{axis} and $\Delta\tau_e$) describe the changes in dynamics upon ligand binding. For instance, a $\Delta S^2_{axis} > 0$ ($\Delta S^2_{axis} = S^2_{axis,complex} - S^2_{axis,apo}$) for a methyl group signifies a decrease in fast timescale motions, whereas a $\Delta S^2_{axis} < 0$ indicates an increase in these motions. We defined a difference in the fitted parameter of >1.5-fold of the propagated error as a significant change in dynamics. Figure 6 shows plots of ΔS^2_{axis} and $\Delta\tau_e$ values versus methyl sequence for the three complexes. We classified three regions with significant ΔS^2_{axis} values into two general groups—those whose dynamics were common to all complexes and those whose dynamics were ligand specific (Figures 6 and 7). For instance, the carboxylate-binding (β1-β2) loop (residues T853–T857) showed increased ΔS^2_{axis} values in all three ligand-bound complexes.

In contrast, two regions in the PDZ domain showed pronounced differences in ΔS^2_{axis} and $\Delta\tau_e$ values among the three complexes. First, the β3 strand and α1 helix region (residues V875–A891) showed positive ΔS^2_{axis} values in both the Caspr4- and SDC1-bound states but not in the pSDC1-bound state (Figures 6 and 7). Specifically, binding to pSDC1 had essentially no effect on S^2_{axis} in this region (the exception being L883$^{\delta1}$). The second affected region was the ligand-binding site (α2 helix and β2 strand). Both SDC1 and pSDC1 binding induced significant ΔS^2_{axis} or $\Delta\tau_e$ in this region of the PDZ domain, specifically at residues L911$^{\delta1,\delta2}$, L915$^{\delta1}$, L920$^{\delta1}$, L922$^{\delta2}$, L923$^{\delta2}$, I846$^{\gamma2}$, I898$^{\gamma2}$, and L862$^{\delta1}$. The motions of the methyl groups in L911$^{\delta1,\delta2}$, L915$^{\delta1}$, L922$^{\delta2}$, and I846$^{\gamma2}$ were more restricted, whereas those of L920$^{\delta1}$, I898$^{\gamma2}$, and L862$^{\delta1}$ became more dynamic. This pattern was distinct from that observed in the PDZ/Caspr4 complex, where residues L915$^{\delta1}$, L920$^{\delta1}$, L922$^{\delta2}$, L923$^{\delta2}$, and I846$^{\gamma2}$ showed no significant ΔS^2_{axis}, but residues L911$^{\delta1,\delta2}$, I898$^{\gamma2}$, and L862$^{\delta1}$ were more restricted on the fast timescale. Thus, the motions of the Tiam1 PDZ domain in the Caspr4-bound state became more restricted, whereas in the SDC1- and pSDC1-bound states the dynamics were heterogeneous with methyl groups showing increased and decreased motions (Figures 6 and 7).

DISCUSSION

Tiam1 is a guanine nucleotide exchange factor for the Rac1 GTPase that plays important roles in cell polarity, cell-cell adhesion, and cell migration. The spatio-temporal dynamics of Tiam1 signaling are tightly regulated by several protein-protein interaction domains. In particular, the PDZ domain interacts with adhesion proteins, such as syndecan1 and Caspr4, and thereby regulates signaling (Shepherd et al., 2010). Here, we identified the binding preferences of this domain for syndecan proteins and defined the structural determinants required for its specificity to several ligands. In addition, we determined the crystal structure of the Tiam1 PDZ domain bound to phosphorylated SDC1 that establishes a paradigm for PDZ/phospholigand interactions. Finally, our analysis of the side-chain dynamics of three Tiam1 PDZ/ligand complexes with very similar binding energetics (ΔG), but distinct entropies, reveals that redistribution of energetics at protein interfaces can have a significant impact on protein dynamics.

Tiam1 PDZ Domain Syndecan Binding Preferences Suggest Biological Signaling Specificity

Previous studies identified PDZ-containing proteins capable of binding syndecan family proteins (Lambaerts et al., 2009). These studies suggest that the C-terminal four amino acids (EFYA) of the PDZ-binding motif are the sole determinants of syndecan binding specificity. However, our previous biochemical and structural analyses of the Tiam1 PDZ domain (Shepherd et al., 2010) and other PDZ/ligand studies (Birrane et al., 2003; Feng et al., 2008; Kozlov et al., 2002; Tyler et al., 2010) demonstrate that residues beyond P_{-3} contribute to peptide ligand recognition. Indeed, our fluorescence-based affinity measurements clearly show that the Tiam1 PDZ domain binds particular syndecans preferentially (affinity for SDC1 and SDC3 peptides ~15-fold greater than that for SDC2 and SCD4 peptides; Table 1). As seen in the Tiam1 PDZ domain/SDC1 structure, residues K912 and N876 in the PDZ domain and the P_{-4} and P_{-6} in syndecans dictate this specificity. The P_{-2} phenylalanine residue may also contribute by stabilizing the EP_{-4} residue and its interaction with K912. Interestingly, the P_{-4} and P_{-6} residues of the Caspr4 peptide are not conserved with those of SDC1 and three isoforms, yet it binds the Tiam1 PDZ domain with the highest affinity of all peptides. The P_{-4} position contains lysine, whereas the P_{-6} has an asparagine, suggesting that the Caspr4 peptide in complex with the PDZ domain assumes a distinct conformation from that seen in SDC1. Although our binding studies were performed with dansyl peptides, the dansyl group does not appear to influence binding specificity as the crystal structure shows it is ~6 Å from KP_{-6} and no additional contacts with the peptide or PDZ domain are apparent. Solution NMR titration experiments with N-terminally acetylated and dansylated pSDC1 peptides indicate that the dansyl group weakly perturbs the chemical shifts of residues in the β2-β3 loop (E866, E867, and D868); however, these residues do not appear to be involved in providing binding specificity for syndecan isoforms (Figure S1).

The residues at position K912 and N876 may also provide specificity in other syndecan-PDZ protein interactions as they vary among other syndecan-binding PDZ domains (Figure 4C). Our results set an important precedent in syndecan biology that PDZ domain proteins can have specificity for individual syndecan receptor proteins. For Tiam1, the PDZ domain

binds SDC1 and mediates cell-matrix and cell-cell adhesion (Shepherd et al., 2010). The data presented here also indicate that Tiam1 couples to SDC3. Interestingly, both Tiam1 and SDC3 have a known function in neurite development, suggesting a potential functional link (Hienola et al., 2006; Miyamoto et al., 2006; Tanaka et al., 2004). Although the specificity of other syndecan-binding PDZ domain pairs has not been determined, our data suggest that other PDZ proteins may also display unique syndecan preferences. Knowledge of this specificity will ultimately be required to decipher the full complement of syndecan interactions and signaling.

Syndecan-PDZ Protein Selection by Ligand Phosphorylation

The phosphorylation of PDZ-binding motifs modulates many PDZ/ligand interactions (Lee and Zheng, 2010). In general, the outcome of phosphorylation is disruption of the interaction, but multiple reports have demonstrated that binding affinity can be enhanced (Adey et al., 2000; Boisguerin et al., 2007; Pangon et al., 2012; Tyler et al., 2010; von Nandelstadh et al., 2009). These studies demonstrate the importance of positive regulation in PDZ/ligand interactions; however, the structural mechanism whereby phosphorylation contributes to the specificity and affinity of PDZ/ligand interactions remains uncharacterized.

We previously determined that SDC1 phosphorylation (at Y309) does not disrupt binding between SDC1 and the Tiam1 PDZ domain (Table 1) (Shepherd et al., 2010). The structures presented here reveal the physical basis for the PDZ/pSDC1 interaction. In short, the Tiam1 PDZ domain has evolved the capacity to bind SDC1 and pSDC1 via distinct mechanisms but with nearly equal affinity (Figures 3 and 4). The structural model and thermodynamic analysis of the Tiam1 PDZ/pSDC1 complex demonstrates that the phosphotyrosine adduct is recognized and stabilized in a phosphoryl binding pocket through electrostatic interactions with residues K879 and T857 of the PDZ domain (Figure 4B). Concomitantly, YP_{-1}-phosphorylation disrupts tyrosine OH interactions with the N876 side chain seen in the PDZ/SDC1 complex resulting in only a small change in affinity between the PDZ/SDC1 and PDZ/pSDC1 complexes. The identity of residues near the phosphoryl binding pocket may provide specificity in other syndecan-binding PDZ domains. Notably, the syntenin1 PDZ2 domain contains a valine (V222) at the equivalent of Tiam1 position 879 and two adjacent aspartic acids (D204 and D224; S851 and T881 in Tiam1, respectively) (Figure 4C). A model of the syntenin1 PDZ2/pSDC1 structure suggests that phosphorylation is electrostatically unfavorable, given that residues D204 and D224 are negatively charged and residue V222 is not basic. Thus, the electrostatic nature of the phosphoryl (S_{-1}) pocket and the β1-β2 loop are likely determinants of whether syndecan phosphorylation enhances binding to a PDZ domain. Based on examination of the amino-acid sequences and electrostatic potential surfaces of other syndecan-binding PDZ domains, we predict that both the synectin and CASK PDZ domains have the capacity to bind YP_{-1}-phosphorylated syndecan ligands in a manner similar to that described here for the Tiam1 PDZ/pSDC1 complex (Figures 4C and S5). Because of the large number of syndecan-binding PDZ proteins, both binding specificity and phosphorylation are likely required to regulate signaling events. Together, our results suggest that amino acids beyond the final four of the C terminus contribute to binding specificity, whereas phosphorylation (at YP_{-1}) contributes

to regulation. For example, both Tiam1 and syntenin bind SDC1 to coordinate cell adhesion but phosphorylation leads to divergent regulation of signaling. For syntenin, phosphorylation disrupts the PDZ2/SDC1 interaction and promotes ectodomain cleavage (Reiland et al., 1996). In contrast, phosphorylation has no effect on the Tiam1 PDZ/SDC1 interaction, leaving Tiam1 available to support further adhesive events via local activation of Rac1. We propose that other syndecan-PDZ protein interactions are regulated in this manner to provide syndecan signaling specificity.

Ligand-Dependent Dynamic Response of the Tiam1 PDZ Domain

Mounting evidence suggests that protein motions or dynamics contribute to affinity, specificity, and allostery in proteins (Frederick et al., 2007; Kay et al., 1996; Korzhnev et al., 2009; Lee et al., 2000; Namanja et al., 2011; Tzeng and Kalodimos, 2011). In this regard, PDZ domains have been excellent model systems (Fuentes et al., 2004; Lockless and Ranganathan, 1999; Petit et al., 2009). Here, we have used the Tiam1 PDZ domain because interactions with several ligands (SDC1, pSDC1, and Caspr4) have been characterized and high-resolution structural data is available (Shepherd and Fuentes, 2011; Shepherd et al., 2010, 2011).

Examination of the ^{15}N backbone dynamics of the ligand-free PDZ domain shows that the β1-β2 and β2- β3 loops exhibit complex motions on the pico- to nanosecond timescale, consistent with the high degree of conformational variability within Tiam1 PDZ structures (Figure 5; Table S2) (Shepherd et al., 2010). Moreover, the free PDZ contains chemical exchange terms (R_{ex}) in the α2 helix, particularly at and near residue K912, which may help accommodate distinct ligands. Upon ligand binding, however, these dynamic regions all become quenched (Figures 5C and S4). Overall, the ^{15}N backbone dynamics of the three PDZ/ligand complexes were very similar but generally unremarkable.

In contrast, the fast timescale motions of side-chain methyl groups in the Tiam1 PDZ domain offer insight into ligand-dependent regulation of dynamics. Changes in side-chain dynamics in the PDZ domain clustered around three distinct areas (Figures 6 and 7). Importantly, the magnitude and direction of the changes in dynamics were different for each of the three complexes. Using the PDZ/SDC1 complex as the reference state, the three regions of significant change in dynamics correspond to the β1-β2 loop, the β3-α1 region, and the peptide-binding site. Motions in both the β1-β2 loop and β3-α1 region became more restricted upon SDC1 binding, whereas changes in dynamics in the peptide-binding site were mixed—some residues becoming more dynamic and others less. The methyl dynamic response in these three regions is reminiscent of those seen in second PDZ domain of the PTP1E phosphatase (PDZ2), where the β3-α1 region corresponds to “distal surface 2” and residues in our current designation of the peptide-binding site encompass both the “peptide-binding site” and “distal surface 1” in PDZ2 (Fuentes et al., 2004). Remarkably, despite having only ~29% identity, these distantly related PDZ domains have very similar dynamic responses upon ligand binding suggesting a conservation of dynamics as seen in free PDZ domains (Law et al., 2009). Moreover, these regions are consistent with the evolutionarily conserved “protein sectors” identified by Ranganathan and colleagues (Halabi et al., 2009).

To probe the dependence of the PDZ dynamic response to individual peptide ligands, we examined two other Tiam1 PDZ/ligand complexes, that is, bound to pSDC1 and to Caspr4. The overall change in methyl dynamics for the Tiam1 PDZ/Caspr4 complex was similar to that of the SDC1 complex. Nevertheless, there was a significant difference: residues L920, I898, and L862 in the peptide-binding site (α2 and β2 regions) were no longer more dynamic. Rather, motions in the entire PDZ domain were quenched. Interestingly, the α2 region is critical for Tiam1 and Tiam2 PDZ domain specificity (Shepherd and Fuentes, 2011; Shepherd et al., 2011), suggesting that dynamics, affinity, and specificity are correlated in this PDZ domain. Without knowledge of the structure of the Tiam1 PDZ/Caspr4 complex, it is difficult to rationalize the detailed mechanism responsible for this result. One possibility is that the phenylalanine substitution at the C terminus (P_0) of Caspr4 supports efficient packing of side-chain residues into the S_0 pocket, rendering it less dynamic (Figures 6 and 7).

The dynamic response of the side chains upon binding pSDC1 was also similar to that seen with SDC1, with the key exception that the entire β3-α1 region showed no dynamic response to ligand binding. The phosphoryl moiety effectively severed the dynamic coupling between the ligand-binding site and the β3-α1 region. As seen in Figures 3 and 4, the phosphorylation of SDC1 changes the conformation of the pYP_{-1} in the absence of any substantial structural change in either the backbone and or side chains of the PDZ domain. However, subtle local changes in conformation and dynamics occur at the phosphotyrosine-binding site that apparently favors binding of the phosphoryl moiety. In particular, the phosphoryl oxygens interact with both the NZ amino group of K879 and the hydroxyl group of T857. Furthermore, methyl group motions of $T857^{\gamma 2}$ in the β1-β2 loop and $L883^{\delta 1}$ in α1 helix became more restricted upon binding to pSDC1 compared to when bound to SDC1, supporting the notion that the β1-β2 and β3-α1 regions are dynamically linked (Figure 8). Collectively, these data demonstrate that ligand phosphorylation can influence the dynamics of the PDZ domain by regulating the local binding energetics at the PDZ/ligand interface and that not all ligands are equal in their capacity to modulate dynamics. The thermodynamics of the PDZ/peptide interactions also support this idea. As seen in Figure 2, the entropic ($-T\Delta S$) contributions to binding vary widely in the three complexes, suggesting a correlation between dynamics and conformational entropy as seen previously by others (Marlow et al., 2010; Tzeng and Kalodimos, 2012). Here, a direct correspondence between PDZ dynamics and conformational entropy is less clear because of uncertainties in the entropic contribution of the ligands.

Previous studies in PDZ domains suggest specific residues act as hubs for the transmission of “dynamic” signals from the peptide-binding site to distal regions. In particular, studies with the PTP1E PDZ2 domain have shown that residue I20 (analogous to F860 in Tiam1) is critical for transmitting dynamic signals to distal sites (Fuentes et al., 2006) and molecular dynamics studies of PDZ3 of PSD-95 support this conclusion (Ota and Agard, 2005). We postulate that residues F860 and Y858 in the Tiam1 PDZ domain work in concert to regulate the propagation of dynamic signals to distal sites. These residues pack against each other to form the S_0 pocket and connect the β1-β2 loop to the β3-α1 region. Moreover, Y858 packs against both T857 and L883 adjacent to the phosphoryl binding site. Thus, it appears that

two opposing effects regulate the propagation of dynamics upon pSDC1 binding. The default response is triggered by ligand binding and propagated to the β3-α1 region (as seen in SDC1 and Caspr4), but the interaction with the phosphotyrosine opposes this response by dampening the motions in this region. Notably, given that the binding energetics (ΔG) of SDC1 and pSDC1 are very similar, this effect must be derived, in part, from a local redistribution of entropy (ΔS).

Conclusions

This study provides the structural analysis of a PDZ domain bound to a phosphorylated PDZ-binding motif and establishes a paradigm for PDZ/phospholigand interactions. This structure and analyses of other syndecan-binding PDZ proteins suggests that syndecan phosphorylation might have differential effects on PDZ/ligand interactions, providing a means of selecting for particular syndecan-PDZ protein interactions and signaling events (Akiva et al., 2012; Roper et al., 2012). Complementary side-chain dynamics studies of three PDZ/ligand complexes revealed that protein dynamics are finely tuned and sensitive to the distribution of binding energetics throughout the protein/ligand interface. As such, particular “hot spots” such as phosphorylation binding sites are critical for the regulation and transmission of dynamic signals. More generally, our results suggest that subtle changes in structure and energetics, such as those seen in the PDZ/pSDC1 and PDZ/Caspr4 complexes, can evolve to regulate protein dynamics and their coupling to distal regions in proteins, that is, regulation of allsotery. Whether the observed changes in dynamics allosterically regulate PDZ/ligand interactions in the context of full-length Tiam1 is currently unknown. However, one possibility is that the Tiam1 Ras binding domain-PDZ region (RBD-PDZ) functions similar to the Par6 CRIB-PDZ region, where Ras binding to the RBD allosterically regulates PDZ ligand binding energetics. Future experiments will be necessary to probe this intriguing possibility.

EXPERIMENTAL PROCEDURES

Protein Expression and Purification

Wild-type and mutant Tiam1 PDZ domain proteins were expressed and purified as previously described using Ni-chelate and size-exclusion chromatography (Shepherd et al., 2010). Isotopic labeling (^{15}N and $^{15}N,^{13}C$) of the Tiam1 PDZ domain was achieved by growing cells in minimal media containing $^{15}NH_4Cl$ and D-glucose (U-^{13}C-99%). Random, fractionally labeled ^{2}H-methyl protein was produced in minimal media containing $^{15}NH_4Cl$ (99%), D-glucose (U-^{13}C-99%) and 60% $^{2}H_2O$. All PDZ domain mutations were produced using oligonucleotide-directed mutagenesis and verified by DNA sequencing (University of Iowa, DNA Facility).

Synthetic Peptides

Peptides were chemically synthesized and used at >95% purity (GeneScript, Piscataway Township, NJ, USA). Peptides used for NMR and ITC experiments were acetylated at their N terminus, whereas peptides used for fluorescence anisotropy binding assays and crystallography were N-terminally dansylated. Peptide concentrations were determined by absorbance measurements (A_{280}) using their predicted extinction coefficient. Peptide amino-

acid sequences were based on human proteins: SDC1 (residues 303–310), SDC2 (residues 195–202), SDC3 (residues 435–442), SDC4 (residues 191–198), and Caspr4 (residues 1,301–1,308).

In Vitro Binding Measurements and Thermodynamic Analysis

Fluorescence anisotropy was used to monitor the binding of Tiam1 PDZ domain proteins to dansylated peptides. Anisotropy measurements were carried out at 25°C on a Fluorolog3 (Jobin Yvon, Horiba) spectrofluorimeter (γ_{ex} = 340 and γ_{em} = 550 nm). All data collection, fitting, and thermodynamic analyses were performed as previously described (Shepherd and Fuentes, 2011).

Crystallization and Data Collection

Crystallization trials were performed by the hanging-drop vapor diffusion method using 0.75 μl of precipitant and protein (20 mg/ml in 20 mM sodium phosphate and 50 mM NaCl at pH 6.8) in the presence of five molar equivalents of dansylated peptide (N-terminally acetylated peptides did not yield high-quality crystals). Crystals of the Tiam1 PDZ/SDC1 complex formed in 0.1 M MES (pH 6.5), 20% PEG 8000, whereas PDZ/pSDC1 crystals were obtained in 0.1 M sodium acetate, 25% PEG 4000, 8% isopropanol. Prior to data collection, crystals were soaked for ~10 s in mother liquor containing 10% glycerol and were flash-frozen in liquid nitrogen. Diffraction data sets were collected on beamline 4.2.2 at the Advanced Light Source (Berkeley, CA, USA) using a NOIR-1 CCD detector.

Structure Determination and Refinement

Indexing, integration, and scaling were performed using d*TREK (Pflugrath, 1999). The PDZ/SDC1 complex crystallized in space group $P2_1$ with two molecules in the asymmetric unit, whereas the PDZ/pSDC1 complex crystallized in space group $P2_12_12_1$ with one molecule per asymmetric unit. The program MOLREP was used for molecular replacement using the free Tiam1 PDZ domain structure (Protein Data Bank [PDB] ID code 3KZD) as the search model (Vagin and Teplyakov, 1997). Manual model building of the PDZ domain and peptide was carried out in Coot (Emsley and Cowtan, 2004). Further refinement was carried out in REFMAC5 (Vagin et al., 2004). Ramachandran plot and structural statistics were determined using modules within the program Phenix (Afonine et al., 2007). Structural and refinement statistics for both structures are given in Table 2. In the PDZ/SDC1 structure both complexes (chains A and B) had electron density for the bound peptide, but the β1-β2 loop was absent in chain A. Chain B of the PDZ/SDC1 structure was used for all figures and structural comparisons. Structural figures and alignments were performed with PyMOL (v. 1.4).

NMR Spectroscopy

NMR experiments were carried out at 25°C (calibrated with methanol) on Bruker 500 MHz and Varian 600 MHz spectrometers equipped with $^{1}H/^{15}N/^{13}C$ probes and z axis pulsed-field gradients. Tiam1 PDZ/ligand complexes were formed by adding small amounts of concentrated peptide (5 mM) to the PDZ domain until saturation (the final stoichiometry of PDZ to ligand was 1:5). Complexes were lyophilized and resuspended in 90% H_2O/10%

D_2O prior to NMR analysis. All protein NMR samples were used at a concentration of 1 mM in phosphate buffer (20 mM $NaPO_4$, 50 mM NaCl [pH 6.8]).

Backbone and side-chain methyl assignments were obtained using standard triple-resonance experiments. Stereo-specific assignments of prochiral methyl groups were achieved using a 10% ^{13}C-PDZ sample and constant-time ^{13}C-HSQC experiments. NMR data was processed using NMRPipe (Delaglio et al., 1995) and analyzed using NMRView (Johnson and Blevins, 1994).

Standard backbone (^{15}N) relaxation experiments were used to collect amide R_1, R_2, and heteronuclear NOE data at 500 and 600 MHz for free PDZ domain and in complex with Caspr4, SDC1, and pSDC1 (Lee and Wand, 1999). R_1 and R_2 experiments were collected at nine relaxation time points along with three duplicates that were used to estimate parameter uncertainties. R_1 relaxation times ranged from 0.035–1.700 s, and R_2 relaxation times ranged from 0.005–0.172 s. The steady-state heteronuclear ^{15}N-[^1H] NOE experiments were acquired using a total recycle delay of ~5 s with and without a ^1H irradiation period of 4.5 s. The relaxation decay rate (R_1 or R_2) for each resolved amide peak was determined by fitting the maximum peak intensities against relaxation times to a single exponential function using in-house programs.

Side-chain ^2H-methyl relaxation experiments for CH_2D isotopomers were collected for samples containing random fractional ^2H-labeling. Deuterium relaxation experiments [$R_1(^2H)$ and $R_{1\rho}(^2H)$ with automatic correction for I_zC_z contributions] were collected at 500 and 600 MHz (Millet et al., 2002; Namanja et al., 2007). Nine relaxation time points along with three duplicate points were collected for the free PDZ domain, as well as the Caspr4- and SDC1- and pSDC1-bound PDZ complexes. Relaxation rate constants were determined by nonlinear fitting of the data to a single exponential function.

Relaxation Analysis

Backbone and side-chain motions in pico- to nanosecond timescales were characterized using the Lipari-Szabo model free formalism (Lipari and Szabo, 1982). Prior to full analysis of ^{15}N relaxation data, a set of trimmed backbone amides were used to fit the overall rotational correlation time (τ_m) (Tjandra et al., 1995). Global fitting of these data yielded an isotropic τ_m of 6.38, 6.23, 6.29, and 6.33 ns for the free PDZ domain and the SDC1, pSDC1, and Caspr4 complexes, respectively. Rotational tumbling anisotropy was found to be small ($D_{\|}/D_{\perp}$ values ranged from 1.03 to 1.06 for free PDZ domain and PDZ complexes) (Lee et al., 1997). Consequently, an isotropic tumbling model was used for subsequent analyses. Backbone dynamic parameters were fitted to the five standard models using ModelFree (v. 4.1) (Mandel et al., 1995) as implemented in Fast-Modelfree (Cole and Loria, 2003). Similar results were obtained using the Akaike's information criterion (Chen et al., 2004). In all, 81/88, 83/88, 83/88, and 82/88 nonproline amides were analyzed for the free, SDC1-, pSDC1-, and Caspr4-bound Tiam1 PDZ domains, respectively.

S^2_{axis} and τ_e for side-chain methyl groups were determined by fitting the relaxation data using the program Relxn2.2 (Lee et al., 1999). Errors in the fitted parameters were estimated using Monte Carlo simulations. The final analysis yielded S^2_{axis} and τ_e parameters for 54/56,

50/56, 50/56, and 48/56 methyl groups for the free PDZ domain, SDC1-, pSDC1-, and Caspr4 complexes, respectively.

Supplementary Material

Refer to Web version on PubMed Central for supplementary material.

Acknowledgments

The authors thank members of the Fuentes lab for helpful discussions and comments on the manuscript. We are grateful to Dr. Lokesh Gakhar for crystallography advice and Drs. Liping Yu and Andrew Fowler for assistance with collection of NMR data. The Roy J. Carver Charitable Trust is acknowledged for continued funding of the College of Medicine NMR Facility. These studies were supported by American Heart Association grants to X.L. (E155500) and E.J.F. (0835261N). The NSF-RIG award (MCB 0918807) to E.J.F. provided initial funding for this project. T.R.S. was supported in part by a National Institutes of Health graduate training grant in Pharmacology (GM067795) and Biotechnology (GM008365).

References

Adey NB, Huang L, Ormonde PA, Baumgard ML, Pero R, Byreddy DV, Tavtigian SV, Bartel PL. Threonine phosphorylation of the MMAC1/PTEN PDZ binding domain both inhibits and stimulates PDZ binding. Cancer Res. 2000; 60:35–37. [PubMed: 10646847]

Afonine PV, Grosse-Kunstleve RW, Adams PD, Lunin VY, Urzhumtsev A. On macromolecular refinement at subatomic resolution with interatomic scatterers. Acta Crystallogr D Biol Crystallogr. 2007; 63:1194–1197. [PubMed: 18007035]

Akiva E, Friedlander G, Itzhaki Z, Margalit H. A dynamic view of domain-motif interactions. PLoS Comput Biol. 2012; 8:e1002341. [PubMed: 22253583]

Asundi VK, Carey DJ. Phosphorylation of recombinant N-syndecan (syndecan 3) core protein. Biochem Biophys Res Commun. 1997; 240:502–506. [PubMed: 9388509]

Birrane G, Chung J, Ladias JA. Novel mode of ligand recognition by the Erbin PDZ domain. J Biol Chem. 2003; 278:1399–1402. [PubMed: 12444095]

Boisguerin P, Ay B, Radziwill G, Fritz RD, Moelling K, Volkmer R. Characterization of a putative phosphorylation switch: adaptation of SPOT synthesis to analyze PDZ domain regulation mechanisms. ChemBioChem. 2007; 8:2302–2307. [PubMed: 17973281]

Chen J, Brooks CL 3rd, Wright PE. Model-free analysis of protein dynamics: assessment of accuracy and model selection protocols based on molecular dynamics simulation. J Biomol NMR. 2004; 29:243–257. [PubMed: 15213423]

Cohen AR, Woods DF, Marfatia SM, Walther Z, Chishti AH, Anderson JM. Human CASK/LIN-2 binds syndecan-2 and protein 4.1 and localizes to the basolateral membrane of epithelial cells. J Cell Biol. 1998; 142:129–138. [PubMed: 9660868]

Cole R, Loria JP. FAST-Modelfree: a program for rapid automated analysis of solution NMR spin-relaxation data. J Biomol NMR. 2003; 26:203–213. [PubMed: 12766418]

Couchman JR. Transmembrane signaling proteoglycans. Annu Rev Cell Dev Biol. 2010; 26:89–114. [PubMed: 20565253]

De Los Rios P, Cecconi F, Pretre A, Dietler G, Michielin O, Piazza F, Juanico B. Functional dynamics of PDZ binding domains: a normal-mode analysis. Biophys J. 2005; 89:14–21. [PubMed: 15821164]

Delaglio F, Grzesiek S, Vuister GW, Zhu G, Pfeifer J, Bax A. NMRPipe: a multidimensional spectral processing system based on UNIX pipes. J Biomol NMR. 1995; 6:277–293. [PubMed: 8520220]

Dhulesia A, Gsponer J, Vendruscolo M. Mapping of two networks of residues that exhibit structural and dynamical changes upon binding in a PDZ domain protein. J Am Chem Soc. 2008; 130:8931–8939. [PubMed: 18558679]

Emsley P, Cowtan K. Coot: model-building tools for molecular graphics. Acta Crystallogr D Biol Crystallogr. 2004; 60:2126–2132. [PubMed: 15572765]

Ethell IM, Hagihara K, Miura Y, Irie F, Yamaguchi Y. Synbindin, A novel syndecan-2-binding protein in neuronal dendritic spines. J Cell Biol. 2000; 151:53–68. [PubMed: 11018053]

Feng W, Wu H, Chan LN, Zhang M. Par-3-mediated junctional localization of the lipid phosphatase PTEN is required for cell polarity establishment. J Biol Chem. 2008; 283:23440–23449. [PubMed: 18550519]

Frederick KK, Marlow MS, Valentine KG, Wand AJ. Conformational entropy in molecular recognition by proteins. Nature. 2007; 448:325–329. [PubMed: 17637663]

Fuentes EJ, Der CJ, Lee AL. Ligand-dependent dynamics and intramolecular signaling in a PDZ domain. J Mol Biol. 2004; 335:1105–1115. [PubMed: 14698303]

Fuentes EJ, Gilmore SA, Mauldin RV, Lee AL. Evaluation of energetic and dynamic coupling networks in a PDZ domain protein. J Mol Biol. 2006; 364:337–351. [PubMed: 17011581]

Gao Y, Li M, Chen W, Simons M. Synectin, syndecan-4 cytoplasmic domain binding PDZ protein, inhibits cell migration. J Cell Physiol. 2000; 184:373–379. [PubMed: 10911369]

Halabi N, Rivoire O, Leibler S, Ranganathan R. Protein sectors: evolutionary units of three-dimensional structure. Cell. 2009; 138:774–786. [PubMed: 19703402]

Harris BZ, Hillier BJ, Lim WA. Energetic determinants of internal motif recognition by PDZ domains. Biochemistry. 2001; 40:5921–5930. [PubMed: 11352727]

Hienola A, Tumova S, Kulesskiy E, Rauvala H. N-syndecan deficiency impairs neural migration in brain. J Cell Biol. 2006; 174:569–580. [PubMed: 16908672]

Johnson BA, Blevins RA. NMR View: A computer program for the visualization and analysis of NMR data. J Biomol NMR. 1994; 4:603–614. [PubMed: 22911360]

Kang BS, Cooper DR, Jelen F, Devedjiev Y, Derewenda U, Dauter Z, Otlewski J, Derewenda ZS. PDZ tandem of human syntenin: crystal structure and functional properties. Structure. 2003; 11:459–468. [PubMed: 12679023]

Kay LE, Muhandiram DR, Farrow NA, Aubin Y, Forman-Kay JD. Correlation between dynamics and high affinity binding in an SH2 domain interaction. Biochemistry. 1996; 35:361–368. [PubMed: 8555205]

Kong Y, Karplus M. Signaling pathways of PDZ2 domain: a molecular dynamics interaction correlation analysis. Proteins. 2009; 74:145–154. [PubMed: 18618698]

Korzhnev DM, Bezsonova I, Lee S, Chalikian TV, Kay LE. Alternate binding modes for a ubiquitin-SH3 domain interaction studied by NMR spectroscopy. J Mol Biol. 2009; 386:391–405. [PubMed: 19111555]

Kozlov G, Banville D, Gehring K, Ekiel I. Solution structure of the PDZ2 domain from cytosolic human phosphatase hPTP1E complexed with a peptide reveals contribution of the beta2-beta3 loop to PDZ domain-ligand interactions. J Mol Biol. 2002; 320:813–820. [PubMed: 12095257]

Lambaerts K, Wilcox-Adelman SA, Zimmermann P. The signaling mechanisms of syndecan heparan sulfate proteoglycans. Curr Opin Cell Biol. 2009; 21:662–669. [PubMed: 19535238]

Law AB, Fuentes EJ, Lee AL. Conservation of side-chain dynamics within a protein family. J Am Chem Soc. 2009; 131:6322–6323. [PubMed: 19374353]

Lee AL, Wand AJ. Assessing potential bias in the determination of rotational correlation times of proteins by NMR relaxation. J Biomol NMR. 1999; 13:101–112. [PubMed: 10070752]

Lee HJ, Zheng JJ. PDZ domains and their binding partners: structure, specificity, and modification. Cell Commun Signal. 2010; 8:1–18. [PubMed: 20181064]

Lee LK, Rance M, Chazin WJ, Palmer AG 3rd. Rotational diffusion anisotropy of proteins from simultaneous analysis of ^{15}N and $^{13}C^{\alpha}$ nuclear spin relaxation. J Biomol NMR. 1997; 9:287–298. [PubMed: 9204557]

Lee AL, Flynn PF, Wand AJ. Comparison of ^{2}H and ^{13}C NMR relaxation techniques for the study of protein methyl group dynamics in solution. J Am Chem Soc. 1999; 121:2891–2902.

Lee AL, Kinnear SA, Wand AJ. Redistribution and loss of side chain entropy upon formation of a calmodulin-peptide complex. Nat Struct Biol. 2000; 7:72–77. [PubMed: 10625431]

Lipari G, Szabo A. Model-free approach to the interpretation of nuclear magnetic resonance relaxation in macromolecules: 1. Theory and range of validity. J Am Chem Soc. 1982; 104:4546–4559.

Lockless SW, Ranganathan R. Evolutionarily conserved pathways of energetic connectivity in protein families. Science. 1999; 286:295–299. [PubMed: 10514373]

Makhatadze GI, Loladze VV, Ermolenko DN, Chen X, Thomas ST. Contribution of surface salt bridges to protein stability: guidelines for protein engineering. J Mol Biol. 2003; 327:1135–1148. [PubMed: 12662936]

Malliri A, van Es S, Huveneers S, Collard JG. The Rac exchange factor Tiam1 is required for the establishment and maintenance of cadherin-based adhesions. J Biol Chem. 2004; 279:30092–30098. [PubMed: 15138270]

Mandel AM, Akke M, Palmer AG 3rd. Backbone dynamics of Escherichia coli ribonuclease HI: correlations with structure and function in an active enzyme. J Mol Biol. 1995; 246:144–163. [PubMed: 7531772]

Marlow MS, Dogan J, Frederick KK, Valentine KG, Wand AJ. The role of conformational entropy in molecular recognition by calmodulin. Nat Chem Biol. 2010; 6:352–358. [PubMed: 20383153]

Masuda M, Maruyama T, Ohta T, Ito A, Hayashi T, Tsukasaki K, Kamihira S, Yamaoka S, Hoshino H, Yoshida T, et al. CADM1 interacts with Tiam1 and promotes invasive phenotype of human T-cell leukemia virus type I-transformed cells and adult T-cell leukemia cells. J Biol Chem. 2010; 285:15511–15522. [PubMed: 20215110]

Mertens AE, Rygiel TP, Olivo C, van der Kammen R, Collard JG. The Rac activator Tiam1 controls tight junction biogenesis in keratinocytes through binding to and activation of the Par polarity complex. J Cell Biol. 2005; 170:1029–1037. [PubMed: 16186252]

Millet O, Muhandiram DR, Skrynnikov NR, Kay LE. Deuterium spin probes of side-chain dynamics in proteins. 1 Measurement of five relaxation rates per deuteron in ^{13}C-labeled and fractionally $^{(2)}$H-enriched proteins in solution. J Am Chem Soc. 2002; 124:6439–6448. [PubMed: 12033875]

Miyamoto Y, Yamauchi J, Tanoue A, Wu C, Mobley WC. TrkB binds and tyrosine-phosphorylates Tiam1, leading to activation of Rac1 and induction of changes in cellular morphology. Proc Natl Acad Sci USA. 2006; 103:10444–10449. [PubMed: 16801538]

Namanja AT, Peng T, Zintsmaster JS, Elson AC, Shakour MG, Peng JW. Substrate recognition reduces side-chain flexibility for conserved hydrophobic residues in human Pin1. Structure. 2007; 15:313–327. [PubMed: 17355867]

Namanja AT, Wang XJ, Xu B, Mercedes-Camacho AY, Wilson KA, Etzkorn FA, Peng JW. Stereospecific gating of functional motions in Pin1. Proc Natl Acad Sci USA. 2011; 108:12289–12294. [PubMed: 21746900]

Nishimura T, Yamaguchi T, Kato K, Yoshizawa M, Nabeshima Y, Ohno S, Hoshino M, Kaibuchi K. PAR-6-PAR-3 mediates Cdc42-induced Rac activation through the Rac GEFs STEF/Tiam1. Nat Cell Biol. 2005; 7:270–277. [PubMed: 15723051]

Ota N, Agard DA. Intramolecular signaling pathways revealed by modeling anisotropic thermal diffusion. J Mol Biol. 2005; 351:345–354. [PubMed: 16005893]

Ott VL, Rapraeger AC. Tyrosine phosphorylation of syndecan-1 and -4 cytoplasmic domains in adherent B82 fibroblasts. J Biol Chem. 1998; 273:35291–35298. [PubMed: 9857070]

Pangon L, Van Kralingen C, Abas M, Daly RJ, Musgrove EA, Kohonen-Corish MR. The PDZ-binding motif of MCC is phosphorylated at position -1 and controls lamellipodia formation in colon epithelial cells. Biochim Biophys Acta. 2012; 1823:1058–1067. [PubMed: 22480440]

Petit CM, Zhang J, Sapienza PJ, Fuentes EJ, Lee AL. Hidden dynamic allostery in a PDZ domain. Proc Natl Acad Sci USA. 2009; 106:18249–18254. [PubMed: 19828436]

Pflugrath JW. The finer things in X-ray diffraction data collection. Acta Crystallogr D Biol Crystallogr. 1999; 55:1718–1725. [PubMed: 10531521]

Reiland J, Ott VL, Lebakken CS, Yeaman C, McCarthy J, Rapraeger AC. Pervanadate activation of intracellular kinases leads to tyrosine phosphorylation and shedding of syndecan-1. Biochem J. 1996; 319:39–47. [PubMed: 8870647]

Roper JA, Williamson RC, Bass MD. Syndecan and integrin interactomes: large complexes in small spaces. Curr Opin Struct Biol. 2012; 22:583–590. [PubMed: 22841476]

Shepherd TR, Fuentes EJ. Structural and thermodynamic analysis of PDZ-ligand interactions. Methods Enzymol. 2011; 488:81–100. [PubMed: 21195225]

Shepherd TR, Klaus SM, Liu X, Ramaswamy S, DeMali KA, Fuentes EJ. The Tiam1 PDZ domain couples to Syndecan1 and promotes cell-matrix adhesion. J Mol Biol. 2010; 398:730–746. [PubMed: 20361982]

Shepherd TR, Hard RL, Murray AM, Pei D, Fuentes EJ. Distinct ligand specificity of the Tiam1 and Tiam2 PDZ domains. Biochemistry. 2011; 50:1296–1308. [PubMed: 21192692]

Sulka B, Lortat-Jacob H, Terreux R, Letourneur F, Rousselle P. Tyrosine dephosphorylation of the syndecan-1 PDZ binding domain regulates syntenin-1 recruitment. J Biol Chem. 2009; 284:10659–10671. [PubMed: 19228696]

Tanaka M, Ohashi R, Nakamura R, Shinmura K, Kamo T, Sakai R, Sugimura H. Tiam1 mediates neurite outgrowth induced by ephrin-B1 and EphA2. EMBO J. 2004; 23:1075–1088. [PubMed: 14988728]

Tjandra N, Feller SE, Pastor RW, Bax A. Rotational diffusion anisotropy of human ubiquitin from ^{15}N NMR relaxation. J Am Chem Soc. 1995; 117:12562–12566.

Tyler RC, Peterson FC, Volkman BF. Distal interactions within the par3-VE-cadherin complex. Biochemistry. 2010; 49:951–957. [PubMed: 20047332]

Tzeng SR, Kalodimos CG. Protein dynamics and allostery: an NMR view. Curr Opin Struct Biol. 2011; 21:62–67. [PubMed: 21109422]

Tzeng SR, Kalodimos CG. Protein activity regulation by conformational entropy. Nature. 2012; 488:236–240. [PubMed: 22801505]

Vagin A, Teplyakov A. MOLREP: an automated program for molecular replacement. J Appl Cryst. 1997; 30:1022–1025.

Vagin AA, Steiner RA, Lebedev AA, Potterton L, McNicholas S, Long F, Murshudov GN. REFMAC5 dictionary: organization of prior chemical knowledge and guidelines for its use. Acta Crystallogr D Biol Crystallogr. 2004; 60:2184–2195. [PubMed: 15572771]

von Nandelstadh P, Ismail M, Gardin C, Suila H, Zara I, Belgrano A, Valle G, Carpen O, Faulkner G. A class III PDZ binding motif in the myotilin and FATZ families binds enigma family proteins: a common link for Z-disc myopathies. Mol Cell Biol. 2009; 29:822–834. [PubMed: 19047374]

Whitney DS, Peterson FC, Volkman BF. A conformational switch in the CRIB-PDZ module of Par-6. Structure. 2011; 19:1711–1722. [PubMed: 22078569]

Zhang H, Macara IG. The polarity protein PAR-3 and TIAM1 cooperate in dendritic spine morphogenesis. Nat Cell Biol. 2006; 8:227–237. [PubMed: 16474385]

Zimmermann P, Tomatis D, Rosas M, Grootjans J, Leenaerts I, Degeest G, Reekmans G, Coomans C, David G. Characterization of syntenin, a syndecan-binding PDZ protein, as a component of cell adhesion sites and microfilaments. Mol Biol Cell. 2001; 12:339–350. [PubMed: 11179419]

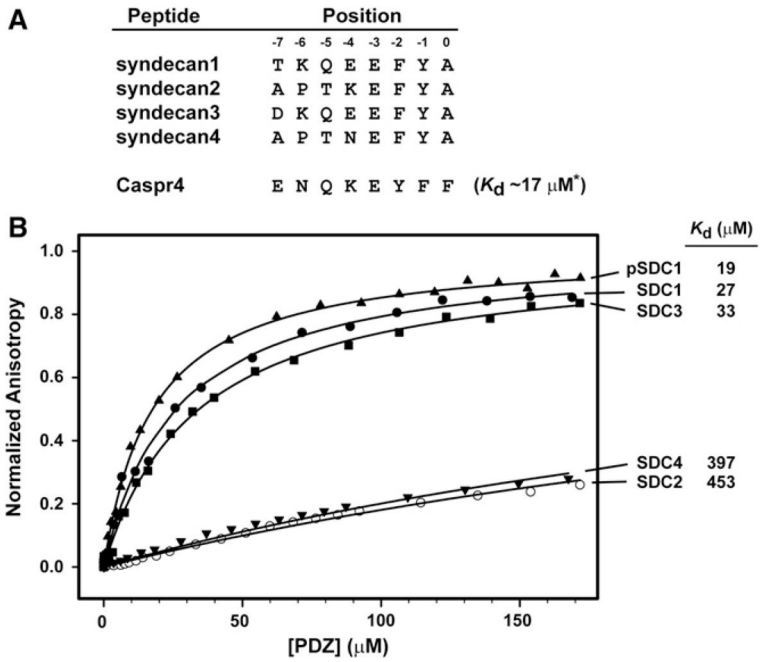

Figure 1. Tiam1 PDZ Domain Binding Affinity for Syndecan Family Proteins

(A) The C termini (C2 region) of syndecan family members and Caspr4.

(B) Representative binding curves for the interaction between the Tiam1 PDZ domain and dansylated peptides derived from phosph-syndecan1 (▲), syn-decan1 (●), syndecan2 (○), syndecan3 (■), and syndecan4 (▼). *Data taken from Shepherd et al. (2010).

A

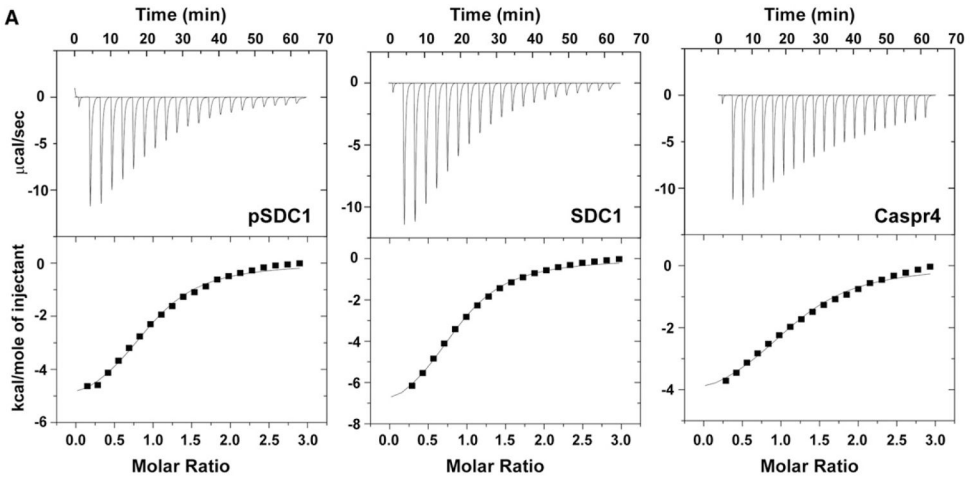

B

Ligand*	ΔH (kcal/mol)	$-T\Delta S$ (kcal/mol)	K_d(μM)	n
pSDC1	-5.67 ± 0.21	-0.41 ± 0.02	35.1 ± 1.4	0.97
SDC1	-8.06 ± 0.30	2.20 ± 0.23	51.8 ± 2.7	0.93
Caspr4	-1.56 ± 0.17	-4.53 ± 0.17	33.8 ± 1.2	0.96

*N-terminally acetylated peptides were used in these experiments.

Figure 2. Thermodynamic Parameters of Tiam1 PDZ/Peptide Interactions Determined by ITC

(A) Thermograms and integrated titration curves are shown for phosphorylated syndecan1 (left panel), syndecan1 (middle panel), and Caspr4 (right panel).

(B) Thermodynamic parameters for PDZ/peptide interactions at 25°C. The change in enthalpy (ΔH), association constant (K_a), and stoichiometry (n) were fit by nonlinear least squares analysis using a single-site binding model in ORIGIN software. The reported thermodynamics parameters are the average of three individual experiments.

See also Figure S1 and Supplemental Experimental Procedures.

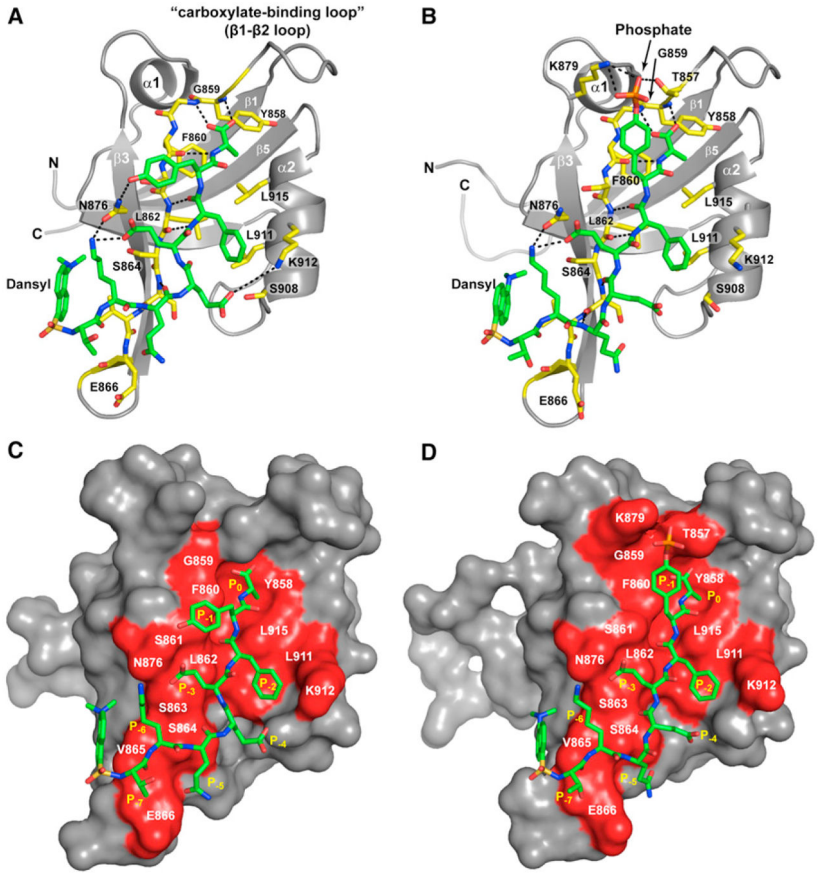

Figure 3. Structures of the Tiam1 PDZ Domain Bound to Syndecan1 and Phospho-Syndecan1

(A and B) Stick models showing side-chain and backbone interactions in the Tiam1 PDZ/SDC1 and PDZ/pSDC1 complexes, respectively. PDZ-domain residues involved in peptide binding are labeled and colored yellow. Dotted lines indicate hydrogen-bond interactions. (C and D) Space-filling models of the Tiam1 PDZ domain bound to SDC1 and pSDC1 peptides (shown as stick models), respectively. The peptide is colored green; PDZ-domain residues involved in peptide binding are labeled and colored red.

See also Table S2 and Figures S1 and S2.

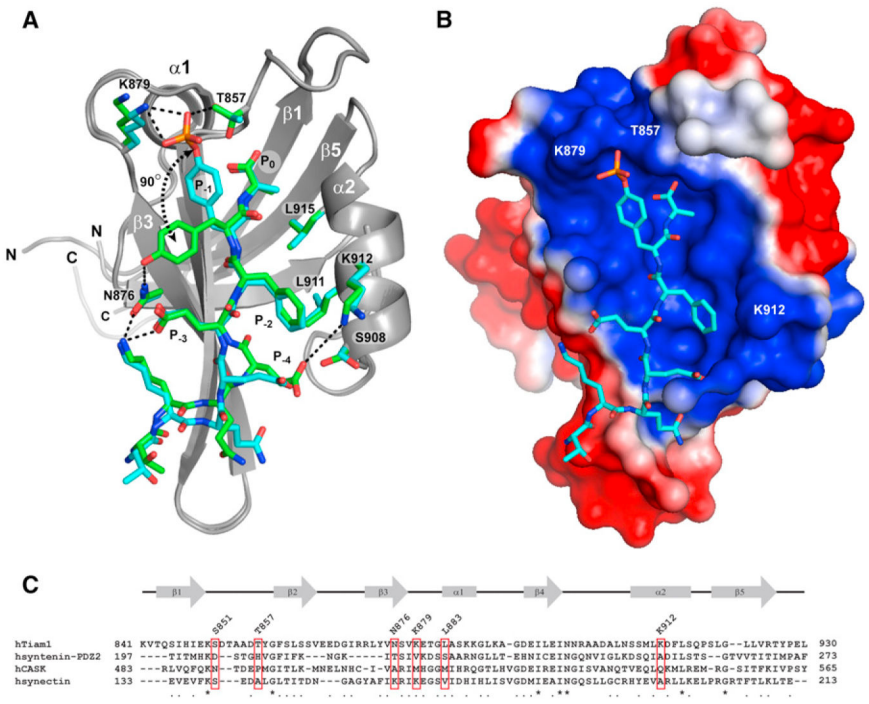

Figure 4. Structural Features of the pSDC1 Phosphotyrosine Binding Pocket

(A) The structures of the Tiam1 PDZ domain (gray) bound to SDC1 (green) or pSDC1 (cyan) are overlaid. Side chains involved in forming the S_{-1} and S_{-2} binding pockets are represented as stick lines. This view highlights the 90° rotation of the P_{-1} tyrosine upon phosphorylation.

(B) The electrostatic potential surface of the PDZ domain in the Tiam1 PDZ/pSDC1 complex. The electrostatic surface is colored continuously from red to blue (−1.0 to +1.0 keV). The electrostatic potential calculation was performed in PyMol (v1.4) using the APBS module.

(C) Structure-based amino acid alignment of PDZ domains that bind to syndecan proteins. See also Table S2 and Figure S5.

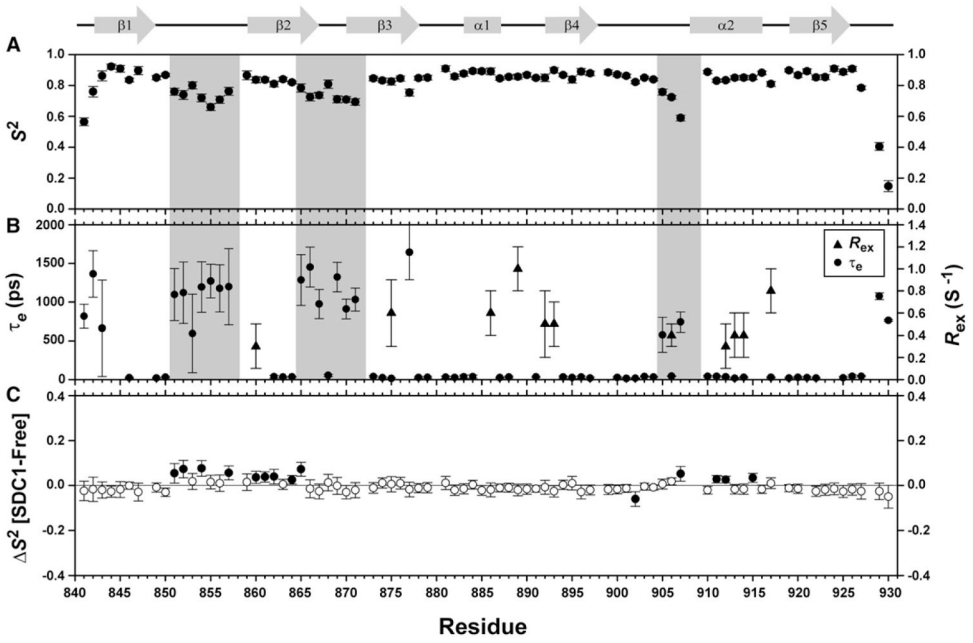

Figure 5. The Pico- to Nanosecond Timescale Dynamics of the Free Tiam1 PDZ-Domain Main Chain and Its Response to Syndecan1 Binding

(A and B) The order parameter (S^2), timescale of motion (τ_e, ●), and chemical exchange (R_{ex}, ▲) of the free Tiam1 PDZ domain plotted for amides along the backbone. Arrows (β strand) and rectangles (α helix) indicate secondary structure of the PDZ domain. Error bars represent the uncertainty as derived from Monte Carlo simulations.

(C) The change in backbone order parameter (ΔS^2) caused by SDC1 binding. Residues that experience significant changes in this parameter are colored black.

See also Figures S3 and S4.

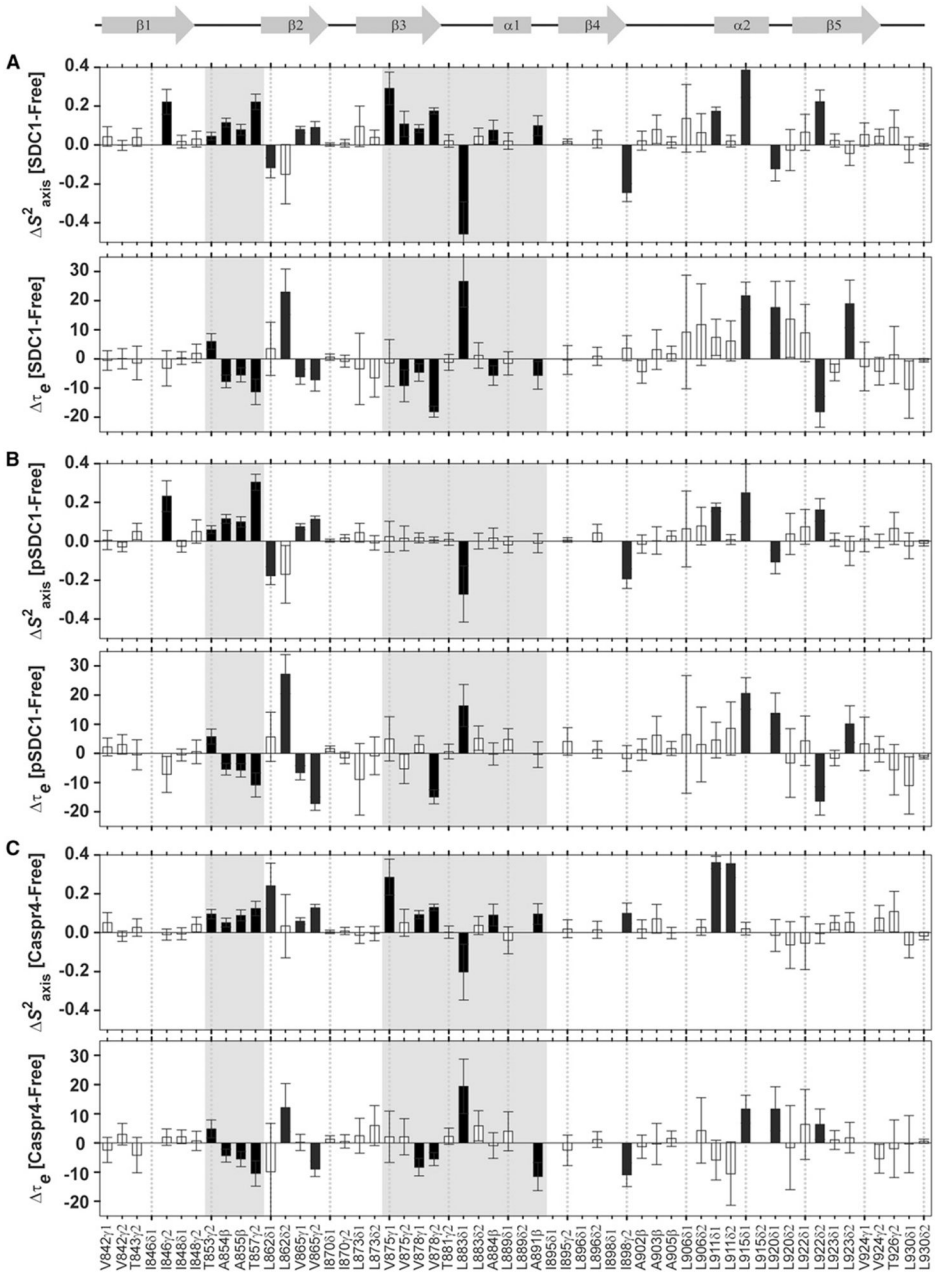

Figure 6. Dynamics of the Methyl Side Chains of Tiam1 PDZ Domain Complexes

(A) The change in S^2_{axis} and τ_e caused by SDC1-binding.

(B) The change in S^2_{axis} and τ_e caused by pSDC1-binding.

(C) The change in S^2_{axis} and τ_e caused by Caspr4-binding.

Three regions that showed significant changes in ΔS^2_{axis} ($\Delta S^2_{axis} = S^2_{axis,bound} - S^2_{axis,apo}$) and $\Delta\tau_e$ ($\Delta\tau_e = \tau_{e,bound} - \tau_{e,apo}$) were the β1-β2 loop (i.e., carboxylate-binding loop) (shaded gray), the β3-α1 region (shaded gray), and the peptide-binding site (the remaining black bars). The error bars represent propagated uncertainty, as derived from Monte Carlo simulations.

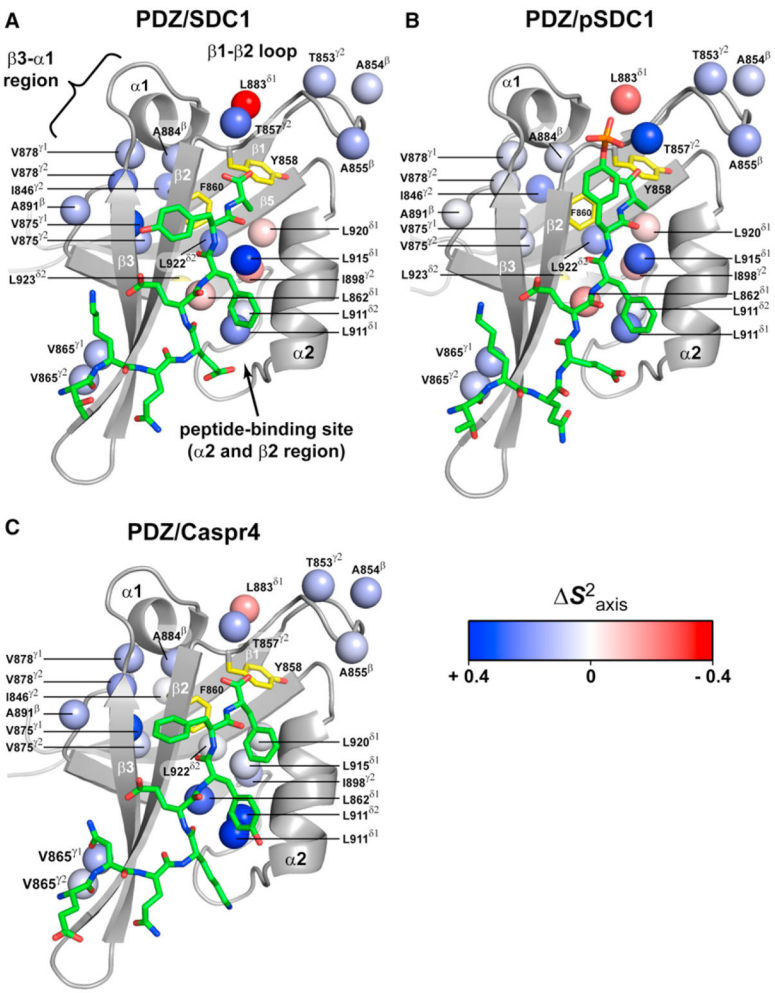

Figure 7. Distinct Dynamics Responses of Methyl Groups of Tiam1 PDZ/Ligand Complexes

(A–C) Side-chain methyl groups with significant changes in dynamics parameters are mapped onto structural models of the PDZ/SDC1, PDZ/pSDC1, and PDZ/Caspr4 complexes, respectively. The methyl groups (spheres) are colored in a continuous gradient from red to blue, with their intensity scaling to the magnitude of ΔS^2_{axis}. Methyl groups colored yellow had a significant $\Delta\tau_e$. The PDZ/SDC1 crystal structure was used as a template to model the PDZ/Caspr4 complex. Residues Y858 and F860 discussed in the text are colored yellow and shown as sticks.

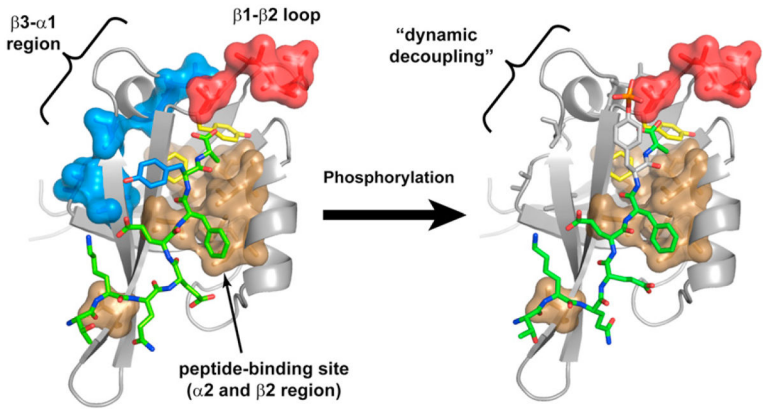

Figure 8. A Model Depicting Ligand-Dependent Dynamic Communication between Regions in the Tiam1 PDZ Domain

The left panel shows the Tiam1 PDZ/SDC1 structure and the three regions whose dynamics were perturbed upon ligand binding (red, β1-β2 loop; blue, β3-α1 region; gold, SDC1-binding site). Phosphorylation of the SDC1 P_{-1} tyrosine residue induces a conformational change that flips this residue into a groove at the junction of α1 helix and the β1-β2 loop (right panel). The conformational switch decouples the dynamics in the β3-α1 region from those at the ligand-binding site.

Table 1

Dissociation Constants for Tiam1 PDZ Domain Interactions with Syndecan Family Ligands

Protein	Peptide	Sequence	K_d (μM)	Fold Change
WT	Caspr4	Dan-ENQKEYFF$_{COOH}$	16.8 ± 5.4[a]	
WT	SDC1	Dan-TKQEEFYA$_{COOH}$	26.9 ± 0.9	1.0[a,b]
WT	SDC2	Dan-APTKEFYA$_{COOH}$	453 ± 22	17[b]
WT	SDC3	Dan-DKQEEFYA$_{COOH}$	33.4 ± 1.9	1.2[b]
WT	SDC4	Dan-APTNEFYA$_{COOH}$	397 ± 17	15[b]
WT	SDC1 (EP$_{-4}$K)	Dan-TKQKEFYA$_{COOH}$	106 ± 7	4.0[b]
PDZ K912E	SDC1	Dan-TKQEEFYA$_{COOH}$	135 ± 23	5.0[b]
PDZ K912E	SDC1 (EP$_{-4}$K)	Dan-TKQKEFYA$_{COOH}$	361 ± 22	13[b]
WT	pSDC1	Dan-TKQEEFYpA$_{COOH}$	19.3 ± 1.5[a]	0.7[b]
PDZ K879E	SDC1	Dan-TKQEEFYA$_{COOH}$	64.7 ± 0.9	2.4[b]
PDZ K879E	pSDC1	Dan-TKQEEFYpA$_{COOH}$	170 ± 6	8.7[c]

Dan, dansyl moiety. See also Table S1.

[a] Taken from (Shepherd et al., 2010).

[b] Fold change versus SDC1 peptide refers to K_d (peptide)/K_d (SDC1).

[c] Fold change versus pSDC1 peptide refers to K_d (peptide)/K_d (pSDC1).

Table 2

Crystallographic Data and Refinement Statistics

	PDZ/SDC1	PDZ/pSDC1
Data Collection Statistics		
Temperature (K)	100	100
Wavelength (Å)	1.000	1.000
Space group	$P2_1$	$P2_12_12_1$
Unit cell parameters		
a, b, c (Å)	26.52, 58.11, 50.95	26.72, 50.14, 57.71
α, β, γ (°)	90.0, 90.5, 90.0	90.0, 90.0, 90.0
Molecules per asymmetric unit	2	1
Resolution range (Å)	38.31–1.85 (1.92–1.85)[a]	37.85–1.54 (1.62–1.54)
I/σ(I)	8.9 (2.7)	34.4 (9.3)
Completeness (%)	99.6 (99.3)	95.5 (74.6)
R_{merge} (%)[b]	7.0 (35.5)	3.0 (12.1)
Redundancy	3.00 (2.91)	6.6 (3.8)
Refinement Details		
Resolution (Å)	1.85	1.54
R_{work}/R_{free} (%)[c]	19.60/24.30	16.55/19.96
Number of atoms		
Protein (peptide)	1,296 (164)	711 (92)
Water	101	95
B-factor average (Å ^{2})		
Protein (main chain)	28.9 (26.4)	11.8 (10.5)
Peptide (dansyl)	34.0 (48.7)	13.8 (15.6)
Water	34.8	26.5
Rmsd from Ideal Geometry		
Bond lengths (Å)	0.022	0.013
Bond angles (°)	2.329	1.431
Dihedral angles (°)	14.30	15.01
Planarity (°)	0.018	0.016
Chirality (°)	0.147	0.116
Ramachandran Plot (% Residues)		
Most favored	98.33	97.94
Additionally allowed	1.67	2.06
Disallowed	0	0

Rmsd, root-mean-square deviation.

[a] Values in parentheses are for the highest resolution shell. One crystal was used for each data collection.

[b] $R_{merge} = \Sigma|I_i - \langle I\rangle|/\Sigma I_i$, where I_i is the intensity of the i^{th} observation, and $\langle I\rangle$ is the mean intensity of the reflections.

[c] $R = \Sigma|F_{obs} - F_{calc}|/\Sigma|F_{obs}|$, crystallographic R-factor, where all reflections belong to a test set of randomly selected data.